



HAL
open science

Terahertz Permittivity of Pressed ZnO and CuO Powder in Polyethylene Pellets: Effect of Porosity

Jaume Calvo-de La Rosa, A. Locquet, Denis Bouscaud, Sophie Berveiller,
David Citrin

► **To cite this version:**

Jaume Calvo-de La Rosa, A. Locquet, Denis Bouscaud, Sophie Berveiller, David Citrin. Terahertz Permittivity of Pressed ZnO and CuO Powder in Polyethylene Pellets: Effect of Porosity. *IEEE Transactions on Terahertz Science and Technology*, 2021, 11 (4), pp.402-407. 10.1109/TTHZ.2021.3063804 . hal-03450727

HAL Id: hal-03450727

<https://hal.science/hal-03450727>

Submitted on 26 Nov 2021

HAL is a multi-disciplinary open access archive for the deposit and dissemination of scientific research documents, whether they are published or not. The documents may come from teaching and research institutions in France or abroad, or from public or private research centers.

L'archive ouverte pluridisciplinaire **HAL**, est destinée au dépôt et à la diffusion de documents scientifiques de niveau recherche, publiés ou non, émanant des établissements d'enseignement et de recherche français ou étrangers, des laboratoires publics ou privés.

Terahertz permittivity of pressed ZnO and CuO powder in polyethylene pellets: Effect of porosity

Jaume Calvo-de la Rosa, Alexandre Locquet, Denis Bouscaud, Sophie Berveiller, and D.S. Citrin

Abstract— Terahertz (THz) spectroscopy is used to measure permittivity (100 GHz-2.5 THz) of ZnO and CuO powders with low fill factor pressed into pellets in a polyethylene binder. We show that porosity (air) of such pressed pellets has a large effect on effective pellet permittivity (~10 %) and on the extracted permittivity of the oxide constituent (~150 %). We explore a two-step analysis based on sequential application of different effective medium models (EMMs), first to account for the air, and subsequently to extract the oxide’s dielectric properties. We show that the combination of the Vegard’s law and the Maxwell Garnett is the best to account, respectively, for the air and the oxides. In this regard, the capacity that this approach has to adapt to each phase’s physical characteristics by using multiple EMMs is an advantage. The resulting oxide permittivities are significantly larger than previously reported for such pellets as a consequence of the porosity. We find for the real relative permittivities of CuO and ZnO ~12.1 and ~8.9, respectively, in the THz range.

Index Terms—Terahertz (THz) spectroscopy, dielectric properties, porosity effect, effective medium models (EMM).

I. INTRODUCTION

THz time-domain spectroscopy (TDS) is widely used for characterizing oxides, semiconductors, and dielectrics. By studying the THz pulse transmitted through the sample in frequency (ν), one seeks the optical constants of the sample [1]–[5]. Many materials are not readily available as single crystals or are strongly attenuating in the THz regime, so one often must rely on measuring powders dispersed in a transparent binder. Alternatively, the powder itself can be of direct interest. This study explores a methodology to extract the dielectric properties of the powder constituent, focusing on CuO and ZnO, accounting for porosity P , which contributes significantly to the extracted oxide-powder permittivity.

To avoid complete attenuation of the signal, a powder at low fill factor may be dispersed in a THz-transparent medium with

well-known THz properties, and pressed into pellets [6], [7]. A pulsed THz transmission experiment is carried out, and the difference in amplitude $A(\nu)$ and phase $\phi(\nu)$ (with respect to propagation through an equal thickness of air) are studied. $\phi(\nu)$ depends on propagation delay, allowing one to deduce the refractive index n , while $A(\nu)$ is used to deduce the absorption coefficient α ,

$$n(\nu) = 1 + \frac{c}{2\pi\nu d} \phi(\nu), \quad (1)$$

$$\alpha(\nu) = -\frac{2}{d} \ln \left[A(\nu) \frac{(n(\nu)+1)^2}{4n(\nu)} \right], \quad (2)$$

with c the speed of light in vacuo. The extinction coefficient $\kappa = \alpha\lambda_0/(4\pi)$ (λ_0 is the in-vacuo wavelength), the real ε' and imaginary ε'' parts of the complex relative permittivity $\hat{\varepsilon}$ are

$$\varepsilon'(\nu) = n(\nu)^2 - \kappa(\nu)^2 = n(\nu)^2 - \left(\frac{\alpha(\nu)\lambda_0}{4\pi} \right)^2, \quad (3)$$

$$\varepsilon''(\nu) = 2n(\nu)\kappa(\nu) = \frac{\alpha(\nu)n(\nu)\lambda_0}{2\pi}, \quad (4)$$

$\alpha(\nu)$ depends on the relative concentrations of sample powder and host material. The volume ratio of the phases (volume fill factor f_V) is a key parameter to extract the optical constants of the powder from the measured—or *effective*—properties of the mixture. EMMs provide a way to do so. The most basic EMM considers a linear dependence [rule of mixtures or Vegard’s law (V) [8], [9]] giving the effective permittivity of the pellet, $\varepsilon_{eff} = f_V\varepsilon_i + (1 - f_V)\varepsilon_h$, where ε_i and ε_h are the inclusion and host permittivity respectively; the host volume fill factor is $1 - f_V$.

More sophisticated approaches are based on Maxwell–Garnett (MG) [9], [10] and Bruggeman (BG) [11] theories. BG accounts for the modification to the applied electromagnetic field due to the field produced by the electric dipoles associated with the other particles themselves, and thus the total response is to the self-consistent field. MG begins with the Clausius–Mossotti relation, based on the response to the field of a single inclusion, but does not account for the dipole-dipole interactions between inclusions; it starts with the polarizabilities of the atomic constituents [11]–[13]. This is

A. Locquet and D. S. Citrin are with the School of Electrical and Computer Engineering, Georgia Institute of Technology, Atlanta, GA 30332 USA, and also with Georgia Tech-CNRS UMI2958, Georgia Tech Lorraine, 57070, Metz, France (e-mail: alexandre@gatech.edu; david.citrin@ece.gatech.edu).

D. Bouscaud and S. Berveiller are with the Laboratoire d’Étude des Microstructures et de Mécanique des Matériaux LEM3 (UMR CNRS 7239), Université de Lorraine, CNRS, Arts et Métiers Institute of Technology, LEM3, F-57070 Metz, France (e-mail: denis.bouscaud@ensam.eu; sophie.berveiller@ensam.eu).

This paragraph of the first footnote will contain the date on which you submitted your paper for review. It will also contain support information, including sponsor and financial support acknowledgment. For example, “This work was supported in part by the U.S. Department of Commerce under Grant BS123456.”

J. Calvo-de la Rosa, was with the DIOPMA Centre, Department of Materials Science and Physical Chemistry, Faculty of Chemistry, IN2UB, Universitat de Barcelona, 08028 Barcelona, Spain. He is now with the Georgia Tech-CNRS UMI2958, Georgia Tech Lorraine, 57070, Metz, France (e-mail: jaumecalvo@ub.edu).

accurate for low f_V (typically $< 30\%$) [12]. MG and BG lead to, respectively,

$$\left(\frac{\varepsilon_{eff}-\varepsilon_h}{\varepsilon_{eff}+\eta\varepsilon_h}\right) = f_V \left(\frac{\varepsilon_i-\varepsilon_h}{\varepsilon_i+\eta\varepsilon_h}\right), \quad (5)$$

$$f_V \left(\frac{\varepsilon_i-\varepsilon_{eff}}{\varepsilon_i+\eta\varepsilon_{eff}}\right) + (1-f_V) \left(\frac{\varepsilon_h-\varepsilon_{eff}}{\varepsilon_h+\eta\varepsilon_{eff}}\right) = 0, \quad (6)$$

with η a shape factor. Though MG and BG typically assume spherical particles ($\eta = 2$) [12], these expressions are often satisfactory for particles of other geometry if the medium is macroscopically isotropic [13].

MG and BG are widely used in calculating inclusions' optical properties by THz-TDS; however, some air inclusions unavoidably remain in the pellets. This implies the pellet containing the oxide powder in the polyethylene matrix is actually a three-component system. THz techniques have already provided interesting results for studying P in pharmaceuticals [14]–[17]. Due to the low air permittivity ($\varepsilon_r = \varepsilon_0 = 1$), P might play a significant role in determining the measured optical constants, and thus the inferred inclusions' properties. Other works have begun to consider the effect of P . Ref. [18] found differences of 5% in n when applying MG to samples with $P \sim 8\text{--}9\%$. Because MG and BG account for somewhat different physical effects and the inclusion geometry is manifestly not spherical, it is not *a priori* evident which approach, if either, is appropriate. Additionally, one approach might be better to account for the oxide particles, for example, while a different approach might account better for P . We thus implement a two-step approach enabling us to treat the oxide particles and P differently, rather than the possibly *prima facie* obvious approach of applying a single EMM to a three-component system.

II. MATERIALS AND EXPERIMENTAL SETUP

CuO and ZnO powders from Inoxia Ltd. (Cranleigh, UK) were verified for chemical purity and crystal structure by x-ray diffraction. The CuO powder has a tenorite (monoclinic) structure, while ZnO is hexagonal (würtzite). Inducos 13/1 (particle size $< 80\ \mu\text{m}$) polyethylene (PE) powder from Induchem (Volketswil, Switzerland) was used as the matrix in which the oxide powders are dispersed. A 13-mm-diameter evacuable pellet die from Specac was used to fabricate the pellets. The constituents were manually mixed. The mixture was introduced on the pellet die and a compressive force of 25 kN was applied to form pellets.

THz-TDS measurements were performed on a TeraView TPS Spectra 3000. Pellets were placed in a sample holder in N_2 . The bandwidth is $\sim 180\ \text{GHz}$ –3 THz.

III. RESULTS AND DISCUSSION

The pellets' characteristics are summarized in Table I. The weight fill factor f_w (which was used to fabricate the pellets) is related to f_V through the density using $0.95\ \text{g/cm}^3$ for PE, $5.61\ \text{g/cm}^3$ for ZnO, and $6.31\ \text{g/cm}^3$ for CuO. P is estimated by comparing each pellet's experimental (ρ_P^{exp}) and theoretical (ρ_P^{theor}) densities by

$$P(\%) = 100 \left(1 - \frac{\rho_P^{exp}}{\rho_P^{theor}}\right) = 100 \left(1 - \frac{\rho_P^{exp}}{f_V \rho_{incl} + (1-f_V) \rho_{host}}\right). \quad (7)$$

TABLE I
PHYSICAL CHARACTERISTICS OF ALL THE FABRICATED PELLETS. NAMING CONVENTION: INCLUSION_ F_w .

Sample	f_w (%)	f_V (%)	ρ (mg/cm ³)	P (%)	f_V^A (%)
PE_ref	0.0	0.0	0.81	13.8	0.0
CuO_02.5	2.5	0.4	0.81	16.4	0.3
CuO_05.0	5.0	0.8	0.83	16.6	0.7
CuO_07.5	7.5	1.2	0.85	16.4	1.0
CuO_10.0	10.0	1.7	0.87	16.7	1.4
CuO_20.0	20.0	3.6	0.96	16.8	3.0
CuO_30.0	30.0	6.1	1.06	17.4	5.0
CuO_40.0	40.0	9.2	1.17	18.8	7.4
ZnO_02.5	2.5	0.4	0.82	16.0	0.4
ZnO_05.0	5.0	0.9	0.84	15.3	0.8
ZnO_07.5	7.5	1.4	0.84	17.3	1.1
ZnO_10.0	10.0	1.9	0.85	18.0	1.5
ZnO_20.0	20.0	4.1	0.93	19.1	3.3
ZnO_30.0	30.0	6.8	0.99	21.9	5.3
ZnO_40.0	40.0	10.2	1.09	23.7	7.8

Table I shows that $P \sim 16\text{--}24\%$ of pellet volume, suggesting that air must be taken into account. We propose to model the pellets as a ternary (PE+oxide+air), instead as a binary system (PE+oxide). It is therefore necessary to recalculate the f_V of each pellet considering P . That is, f_V represents the oxide content in the ideal PE+oxide system. We now define the *actual volume fill factor* f_V^A , which considers the relative oxide volume (f_V) over the nonporous ($100-P$) volume. This parameter is calculated as $f_V^A(\%) = (100 - P)f_V(\%)$ also in Table I and compared with f_V . Indeed, air occupies a larger volume than the oxide in our samples. This emphasizes the importance of accounting P .

All these samples have been characterized by THz-TDS. THz transmitted signals for all pellets are shown in Fig. 1(a) and (c). Analysis is most easily done in the frequency domain (FD) shown in Fig. 1(b) and (d).

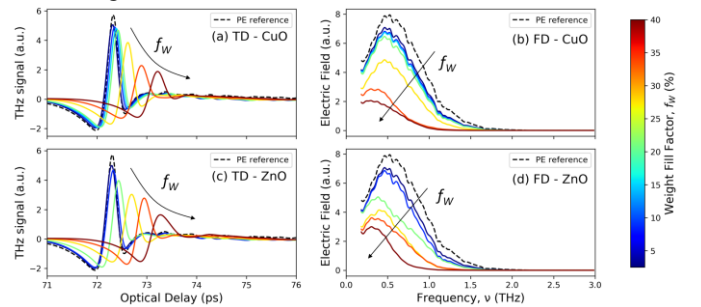


Fig. 1. THz (a) TD and (b) FD signals for CuO, and THz (c) TD and (d) FD signals for ZnO. Both samples consist of oxide particles dispersed in PE pellets for various weight fill factors f_w . Arrows show the tendency with increasing f_w .

As f_w of the oxide powder increases, the propagation delay is seen to increase, i.e., the increasing effective n of the pellet leads to smaller THz group velocity. Also, as f_w increases, the amplitude of the signal reduces because of increasing attenuation.

Once P is quantified and the THz-TDS experiments performed, we explore ways to extract the oxide dielectric properties. The strategy is shown in Fig. 2. Due to the real

permittivity of air ($\hat{\epsilon} = 1 + 0j$), we only compute the real part in the following, as the imaginary part may result in infinite values to compensate the zero contribution from air when applying the EMMs. First, we compute P considering air as the inclusion ($\epsilon^{Air} = \epsilon_i = 1$) and use the measured effective permittivity ($\epsilon_{eff}^{PE+oxide+Air}$) to calculate the permittivity of the solid phase (PE+oxide), corresponding to the host (ϵ_h). Thus, P plays the role of f_v in this first step. The result is therefore the permittivity of a homogeneous solid phase corresponding to the PE+oxide mixture. In Step 2, we use the calculated PE+oxide permittivity as the effective permittivity ($\epsilon_{eff}^{PE+oxide}$), and by using the known value for PE as the host ($\epsilon^{PE} = \epsilon_h = 2.08$) and f_v , the permittivity of the oxide inclusions ($\epsilon_i = \epsilon^{oxide}$) can be extracted. Step 2 is the one typically used [19], [20] and, with Step 1, we are adding a previous step that removes the air from the effective permittivity of the mixture. If one does not want to account for P , Step 1 can be omitted. It must be highlighted that we have done this computation by using all combinations of V, MG, and BG in the two steps.

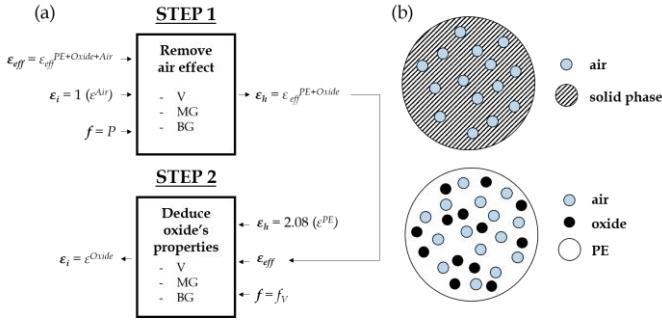


Fig. 2. (a) Two-step method for various EMM combinations, and (b) graphical representation of the phase interpretation at each step.

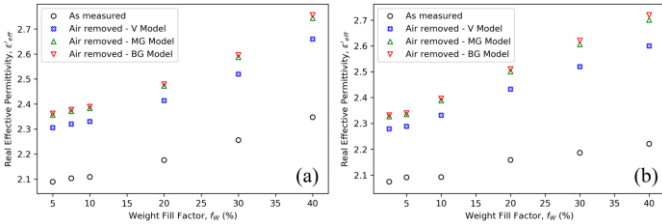


Fig. 3. Comparison of effective permittivity of as-measured data, and that obtained after removing the contribution of P by three EMMs, for (a) CuO and (b) ZnO samples.

The impact of this procedure is seen in Fig. 3, where the values of $\epsilon_{eff}^{PE+oxide}$ obtained from the various EMMs found in Step 1 are plotted along with the raw $\epsilon_{eff}^{PE+oxide+Air}$. A $\sim 10\%$ effect is seen on the effective real permittivity when P is accounted for in all EMMs considered, emphasizing the importance of P . Further, we also observe that the increase in permittivity is larger when MG or BG models are used compared with V. In conclusion, Fig. 2 shows that using Step 1 to account for P is essential, as there is a considerable effect on the permittivity (that is subsequently used to extract the oxide permittivity in Step 2).

In Step 2, we evaluate how this change in effective permittivity influences the calculated oxide permittivity. We look for the inclusions' permittivity ϵ_i (i.e., ϵ^{oxide}) that minimizes the difference between the experimental and the calculated data

at each f_v . We perform this with the four datasets in Fig. 3 as the initial $\epsilon_{eff}^{PE+oxide}$ to deduce the oxide inclusions' properties by means of the three different EMMs. We have therefore computed 12 different combinations of models. The difference between the experimental and the calculated data is evaluated by means of the *fitting error* (FE),

$$FE = \frac{\sum_{s=1}^m (\epsilon_s^{exp} - \epsilon_s^{cal})^2}{m}, \quad (8)$$

with m the number of samples, and ϵ_s^{exp} and ϵ_s^{cal} the experimental and calculated values of the real permittivity. Fits between experimental and calculated values are shown in Fig. 4 for CuO and Fig. 5 for ZnO. The permittivity for $f_v = 100\%$ corresponds to the inclusions' (oxides') calculated permittivity, as obtained by each one of the EMMs.

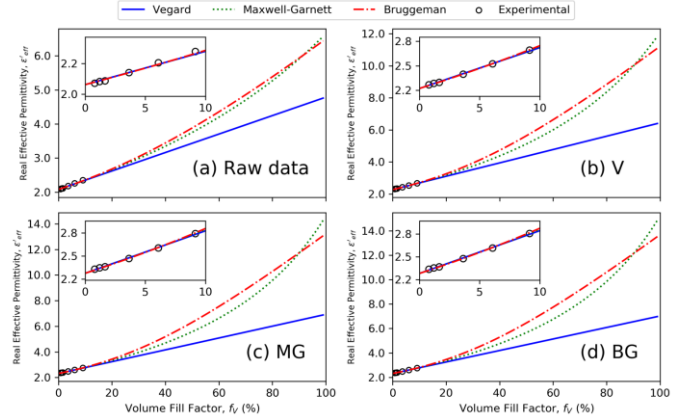


Fig. 4. Comparison between experimental and simulated effective permittivity values for CuO samples by using V, MG, and BG. Calculated values are fitted to effective permittivity calculated by different EMMs: (a) without removing air contribution; (b) V; (c) MG; and (d) BG. Insets show the low f_v region.

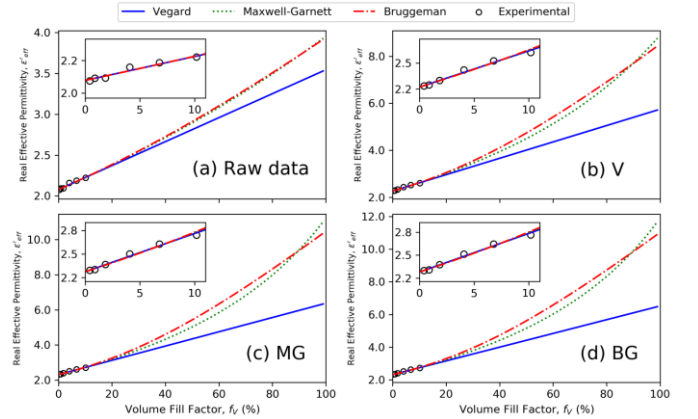


Fig. 5. Comparison between experimental and simulated effective permittivity values for ZnO samples by using V, MG, and BG. Calculated values are fitted to effective permittivity calculated by different EMMs: (a) without removing air contribution; (b) V; (c) MG; and (d) BG. Insets show the low f_v region.

The three models follow the tendencies of the experimental data for lowest f_v . Agreement between calculated and experimental results is excellent in all cases. Though the fit is better for CuO (Fig. 4) than for ZnO (Fig. 5), it is difficult to draw a clear conclusion on the model providing the most accurate results. In order to use an objective criterion, we have compared FE in each case. Table II and Table III provide for

CuO and ZnO, respectively, the calculated permittivity for the oxides and the FE for all EMM combinations.

TABLE II
CuO REAL PERMITTIVITY CALCULATED BY THE VARIOUS EMMs. FE IS SHOWN IN BRACKETS.

		OXIDE MODEL (STEP 2)		
		V	MG	BG
		Air not removed	4.8 [16x10 ⁻⁵]	6.7 [14x10 ⁻⁵]
AIR MODEL (STEP 1)	V	6.4 [3x10 ⁻⁵]	12.1 [2x10 ⁻⁵]	11.2 [2x10 ⁻⁵]
	MG	6.9 [5x10 ⁻⁵]	14.6 [3x10 ⁻⁵]	13.2 [5x10 ⁻⁵]
	BG	7.0 [5x10 ⁻⁵]	15.2 [4x10 ⁻⁵]	13.7 [6x10 ⁻⁵]

From Table II, we observe that CuO permittivity varies with the method used, from 4.8 to 15.2. As expected, the estimated permittivity increases when P is considered. FE is reduced one order of magnitude when P is accounted for, highlighting the importance of Step 1. Though FE is similar when P is considered, we observe that V works well for Step 1, but not for Step 2. The selection of V for deducing P is in excellent agreement with previous works [21]–[23] reporting a linear relationship between P and the dielectric properties in pharmaceuticals. This seems reasonable when considering the physical assumptions of the model: it removes the proportional volumetric contribution of air but does not account for the electric field distributions of the oxide phase. For the latter effect, both MG and BG are more adequate models. Despite similar FE for MG and BG when deducing the inclusions' properties, we consider MG as most appropriate due to the low f_V in our samples ($\leq 10\%$). We conclude that V+MG ($\epsilon' \sim 12.1$) is most self-consistent value, which is compatible with the observed low FE.

TABLE III
ZnO REAL PERMITTIVITY CALCULATED BY THE VARIOUS EMMs. FE IS SHOWN IN BRACKETS.

		OXIDE MODEL (STEP 2)		
		V	MG	BG
		Air not removed	3.5 [1x10 ⁻⁴]	4.0 [1x10 ⁻⁴]
AIR MODEL (STEP 1)	V	5.8 [2x10 ⁻⁴]	8.9 [3x10 ⁻⁴]	8.5 [4x10 ⁻⁴]
	MG	6.4 [3x10 ⁻⁴]	11.2 [4x10 ⁻⁴]	10.5 [5x10 ⁻⁴]
	BG	6.5 [3x10 ⁻⁴]	11.9 [4x10 ⁻⁴]	11.0 [5x10 ⁻⁴]

For ZnO (Table III) FE is larger when P is accounted for. The difference may be due to the larger porosity of the ZnO compared with CuO pellets. Indeed, larger P may imply more scattering, leading the air phase to be inconsistent with the EMMs assumptions. Despite the nonideality of these results, we consider V+MG ($\epsilon' \sim 8.9$) as most self-consistent, following the physical criterion discussed above. Again, this is the approach (of those accounting for P) leading to the lowest FE.

The comparison of our results with literature is not straightforward due to the strong dependence of the optical properties on chemical composition, physical characteristics,

and frequency. We do not consider the optically anisotropy of these crystals which is smaller than the uncertainties in the measurements and analysis. While our approach is self-consistent for a given powder, the inferred optical constants for the powdered material may not be identical with those for the bulk. We have not found published results for the same materials under similar experimental conditions with which we can perform a confident comparison. Indeed, reported results for the same samples and frequency range in Ref. [20] did not account for P . Compared with that work, we find an increase in ϵ' by 124 % for CuO (12.1 vs 5.4) and 147 % (8.9 vs 3.6) for ZnO. The variation in ϵ' is more significant than the one reported in Ref. [18], $\sim 5\%$ in n . This difference might be explained by the larger ϵ' and P ($\sim 8\text{-}9\%$ vs $\sim 13\text{-}24\%$) of our samples. Also, the process used in Ref. [18] consists in a one-step MG calculation. The ability of our method to use different EMMs for each phase is a benefit. In summary, the proposed method provides a way to extract the inclusions' properties by removing the pellet's remaining air effect (accounting for permittivity differences between phases, though not scattering [24]). However, it must be highlighted that the obtained results still correspond to the powder sample (not the bulk) as it does not consider size effects. Additionally, the model incorporating a combination of EMMs provides a framework for predicting powder optical constants in a self-consistent way, over a range of fill factors.

IV. CONCLUSION

The combination of Vegard's law for porosity and Maxwell-Garnett to extract the oxide properties provides the highest degree of self-consistency based on both physical expectations and the minimization of the fitting error. V removes the proportional permittivity of the system due to P , while MG accounts for the electric field distribution of the oxides. It might not be surprising that MG (rather than BG) is best to account for the oxide powder as we are far from any resonance of the system (which might be expected to be the circumstances under which BG is appropriate), while the Clausius-Mossotti relation built into MG captures the essential local-field effects occurring in the neighborhood of the high-permittivity particles in the relatively low permittivity matrix. Thus, this work provides a practical methodology for extracting THz optical constants from data obtained from oxide powder-filled polyethylene pressed pellets with low f_V . Such an approach is crucial for materials with large attenuation constants or when high-quality bulk samples might not be available.

ACKNOWLEDGMENT

Authors acknowledge the financial support of Conseil Régional Grand Est and CPER SusChemProc. Moreover, J. Calvo-de la Rosa acknowledges grant Ajuts a la Docència i a la Recerca (ADR) given by the Universitat de Barcelona and the Catalan Government for the quality accreditation given to his research group DIOPMA (2017 SGR 118).

REFERENCES

- [1] S. R. Ganti, S. K. Sundaram, and J. S. McCloy, "Frequency dependent optical and dielectric properties of zinc sulfide in Terahertz regime," *Infrared Phys. Technol.*, vol. 65, pp. 67–71, 2014.
- [2] I. Takeuchi, M. Otsuki, H. Kuroda, and K. Makino, "Estimation of crystallinity of indomethacin by usage of terahertz time-domain spectroscopy and calibration curve: Correlation between crystallinity and solubility," *J. Drug Deliv. Sci. Technol.*, vol. 45, no. February, pp. 70–75, 2018.
- [3] Q. Wang, X. Li, T. Chang, Q. Hu, and X. Yang, "Terahertz spectroscopic study of aeronautical composite matrix resins with different dielectric properties," *Optik (Stuttg.)*, vol. 168, pp. 101–111, 2018.
- [4] Z. Weng *et al.*, "Microstructure and broadband dielectric properties of Zn₂SiO₄ ceramics with nano-sized TiO₂ addition," *Ceram. Int.*, vol. 45, no. 10, pp. 13251–13256, 2019.
- [5] M. Ma *et al.*, "The dielectric properties of some ceramic substrate materials at terahertz frequencies," *J. Eur. Ceram. Soc.*, vol. 39, no. 14, pp. 4424–4428, 2019.
- [6] T. Bardon, R. K. May, P. F. Taday, and M. Strlič, "Influence of Particle Size on Optical Constants from Pellets Measured with Terahertz Pulsed Spectroscopy," *IEEE Trans. Terahertz Sci. Technol.*, vol. 6, no. 3, pp. 408–413, 2016.
- [7] H. Namkung, J. Kim, H. Chung, and M. A. Arnold, "Impact of pellet thickness on quantitative terahertz spectroscopy of solid samples in a polyethylene matrix," *Anal. Chem.*, vol. 85, no. 7, pp. 3674–3681, 2013.
- [8] S. Mehboob *et al.*, "Terahertz time domain spectroscopy of amorphous and crystalline aluminum oxide nanostructures synthesized by thermal decomposition of AACH," *Mater. Chem. Phys.*, vol. 191, pp. 62–69, 2017.
- [9] J. C. Maxwell Garnett, "Colours in Metal Glasses and in Metallic Films," *R. Soc.*, vol. 203, no. 359–371, pp. 385–420, 1904.
- [10] J. C. Maxwell Garnett, "Colours in Metal Glasses and in Metallic Films in Metallic Solutions - II," *R. Soc.*, vol. 205, no. 387–401, pp. 237–288, 1905.
- [11] D. A. G. Bruggeman, "Calculation of various physics constants in heterogenous substances," *Ann. Phys.*, vol. 24, pp. 636–664, 1935.
- [12] H.-E. Peiponen *et al.*, *Terahertz spectroscopy and imaging*. Springer Series in Optical Sciences The, 2013.
- [13] V. A. Markel, "Introduction to the Maxwell Garnett approximation: tutorial," *J. Opt. Soc. Am. A*, vol. 33, no. 7, p. 1244, 2016.
- [14] Y. C. Shen, "Terahertz pulsed spectroscopy and imaging for pharmaceutical applications: A review," *Int. J. Pharm.*, vol. 417, no. 1–2, pp. 48–60, 2011.
- [15] D. Markl *et al.*, "Fast and non-destructive pore structure analysis using terahertz time-domain spectroscopy," *Int. J. Pharm.*, vol. 537, no. 1–2, pp. 102–110, 2018.
- [16] D. Markl *et al.*, "Characterisation of pore structures of pharmaceutical tablets: A review," *Int. J. Pharm.*, vol. 538, no. 1–2, pp. 188–214, 2018.
- [17] I. Tikhomirov, D. Markl, and M. Naftaly, "Measurements of effective porosity of pharmaceutical tablets using THz TDS," *Int. Conf. Infrared, Millimeter, Terahertz Waves, IRMMW-THz*, vol. 2019-Septe, pp. 1–2, 2019.
- [18] E. P. Parrott, J. A. Zeitler, and L. F. Gladden, "Accurate determination of optical coefficients from chemical samples using terahertz time-domain spectroscopy and effective medium theory," *Opt. Lett.*, vol. 34, no. 23, p. 3722, 2009.
- [19] F. Wan, J. Han, and Z. Zhu, "Dielectric response in ferroelectric BaTiO₃," *Phys. Lett. Sect. A Gen. At. Solid State Phys.*, vol. 372, no. 12, pp. 2137–2140, 2008.
- [20] J. Calvo-de la Rosa, A. Locquet, S. Bouscaud, D. Berveiller, and D. S. Citrin, "Optical Constants of CuO and ZnO Particles in the Terahertz Frequency Range," *Ceram. Int.*, 2020.
- [21] K. E. Peiponen, P. Silfsten, J. Pajander, and J. Ketolainen, "Broadening of a THz pulse as a measure of the porosity of pharmaceutical tablets," *Int. J. Pharm.*, vol. 447, no. 1–2, pp. 7–11, 2013.
- [22] P. Bawuah *et al.*, "Detection of porosity of pharmaceutical compacts by terahertz radiation transmission and light reflection measurement techniques," *Int. J. Pharm.*, vol. 465, no. 1–2, pp. 70–76, 2014.
- [23] P. Bawuah *et al.*, "Terahertz study on porosity and mass fraction of active pharmaceutical ingredient of pharmaceutical tablets," *Eur. J. Pharm. Biopharm.*, vol. 105, pp. 122–133, 2016.
- [24] H. Tuononen, E. Gornov, J. A. Zeitler, J. Aaltonen, and K.-E. Peiponen, "Using modified Kramers–Kronig relations to test transmission spectra of porous media in THz-TDS," *Opt. Lett.*, vol. 35, no. 5, p. 631, 2010.